applied sciences

MDPI

Article

Experimental Study on Shear Creep and Long-Term Strength of Clay-Type Muddy Interlayer

Pengzheng Guo [1], Jiaming Zhang [1,*], Fei Liu [1], Wenlian Liu [2], Zhiqiang Wang [2] and Jipu Chen [1]

1 Faculty of Civil Engineering and Mechanics, Kunming University of Science and Technology, Kunming 650504, China; guopengzheng@stu.kust.edu.cn (P.G.); liufei123@stu.kust.edu.cn (F.L.); cip836@163.com (J.C.)
2 China Nonferrous Metals Industry Kunming Survey and Design Institute Co., Kunming 650051, China; lwenl702@sina.com (W.L.); wzhq83@163.com (Z.W.)
* Correspondence: zhangjiaming@kust.edu.cn

Abstract: In order to have a better understanding of the shear creep characteristics of muddy interlayer in unstable landslides, we took the more "inferior" clay muddy interlayer as the research object, and shear creep experiments under different normal stress levels were carried out by means of hierarchical loading. This paper focuses on the variation law of creep curve and its long-term strength in the clay-type muddy interlayer under different normal stresses. The results showed that the creep characteristics of clay-type muddy interlayer were obvious: at the same normal stress level, instantaneous deformation, initial creep and stable creep appeared at lower shear stress level; at the level of rupture shear stress, there were two cases: the creep curve included three stages of typical initial creep, stable creep and accelerated creep failure, or directly entered the accelerated creep stage until the specimen's failure. The average shear and stable creep rate of the muddy interlayer specimen increased exponentially with the increase in shear stress. The empirical formula $u = u_0 + A\,[1 - \mathrm{e}^{(-Bt)}] + Ct^n$ of shear strength could better reflect the creep deformation law of muddy interlayer, and the correlation coefficient R^2 varies from 0.90 to 0.99. Based on the definition of long-term ultimate strength, the long-term strength of clay-type muddy interlayer was determined.

Keywords: muddy interlayer; clay type; direct shear test; creep characteristics; long-term strength

check for updates

Citation: Guo, P.; Zhang, J.; Liu, F.; Liu, W.; Wang, Z.; Chen, J. Experimental Study on Shear Creep and Long-Term Strength of Clay-Type Muddy Interlayer. *Appl. Sci.* **2023**, *13*, 12151. https://doi.org/10.3390/app132212151

Academic Editor: Syed Minhaj Saleem Kazmi

Received: 3 September 2023
Revised: 4 November 2023
Accepted: 5 November 2023
Published: 8 November 2023

1. Introduction

Muddy interlayer refers to the special weak layer with a loose structure formed by the long-term physical and chemical action of interlayer dislocation and groundwater in rock mass [1,2]. The muddy interlayer has remarkable creep characteristics: the long-term strength is relatively low, and its strength is much lower than that of the upper and lower strata. In engineering rock mass, the strength characteristic of muddy interlayer has a significant time effect, so for the case of a slope with a muddy interlayer, it is easier to form a potential sliding surface and become the key control factor of slope long-term stability [3–5]. It often causes some geological disasters, such as rock-mass instability and rock landslides [5–9]. Many scholars have conducted engineering projects containing muddy interlayer to carry out in-depth research, and achieved important results [10–16]. Therefore, the study of muddy interlayer and weak interlayer has always been the focus of research in the field of engineering geology.

Currently, scholars have conducted comprehensive research on muddy interlayer, including its classification [1,17], formation mechanisms [18] and various experiments and numerical simulation studies involving weak interlayer and muddy interlayer. Zhao et al. [19] based on numerical simulation, analyzed the influence of large-scale CJRM and interlayer shear weak zone on rock mass engineering stability under excavation conditions, and put forward a rock mass stability evaluation method of a large columnar joint interlayer shear weak zone based on BP neural network.

Han et al. [20] conducted a comprehensive study on the engineering geological characteristics of the interlayer shear weak zones at the Baihetan Hydropower Station through geological surveys and laboratory experiments. Zhou et al. [21] introduced a power function to fit the strain–time relationship in the creep process of muddy interlayers, and compared the traditional–isochronous curves to obtain long-term strength; Han et al. [22] explored the creep characteristics of the interlayer mismatch zones through straight shear creep experiments; Tang et al. [23] used the cyclic loading and unloading method to conduct uniaxial compression rheological tests on intact rocks and rock masses under cyclic loading and unloading conditions; Zuo et al. [24] investigated the overall damage behavior of rock–coal–rock assemblages containing weak coal interlayers by uniaxial and triaxial compression tests; Chen et al. [25] investigated the strength and deformation characteristics of tailings specimens containing fine-grained interlayers by undrained shear tests; Ren et al. [26] used cement mortar, gypsum and other rock-like materials to simulate rocks and weak interlayers, and studied the anchorage mechanical properties of rock materials with weak interlayers through uniaxial compression tests; Miao et al. [27] conducted straight shear-creep tests and ring shear tests on two remodeled specimens with different clay content to explore the effect of clay content on landslide evolution; Chen et al. [28] investigated the shear rheological properties of natural weakly structured surfaces of rock bodies through indoor creep tests under different normal stress conditions; and Chen et al. [29], based on the shear creep mechanics test of the interlayer dislocation zone of a high abutment slope rock mass, studied the interlayer dislocation zone shear creep mechanical properties and proposed a creep constitutive equation considering the accelerated creep process. In the construction of underground structures such as tunnel excavation, it is often necessary to consider the interaction between the tunnel lining structure and the surrounding soil [30,31]. Han et al. [32] investigated the load-bearing behavior of tunnel-type anchor rods in underlying soft interlayered soft rocks through on-site model testing and numerical simulation. Ma et al. [33] took the soft interlayer of a potential landslide zone in an open-pit limestone mine in Sichuan Province as the research object, and conducted ring shear test analysis in the various strength and deformation properties of weak interlayers under different water contents and normal stresses.

Scholars have conducted extensive experimental research on muddy interlayers; however, there is a lack of research on "lower-quality" classifications within muddy interlayers, such as clay-type muddy interlayers. A clay-type muddy interlayer is defined as having a clay content greater than 20%, a gravel content less than 10%, and the sum of gravel and sandy particles greater than fine particles [1]. Clay-type muddy interlayers further develop from the formation of muddy interlayers and can gradually evolve into multiple layers. Its degree of clay mineralization is high, making creep more likely to occur. As a unique type of muddy interlayer, they possess representativeness and research value. Yi et al. [3] reported that muddy interlayers are widely distributed in the red bed regions of Southwest China. They are the poorest engineering features in rock masses on slopes and are critical factors in controlling geological hazards in the red bed regions of Southwest China. Muddy interlayers often lead to various engineering geological problems and, therefore, studying them is of significant engineering importance. In the long-term creep process of clay-type muddy interlayers within slopes containing multiple layers of muddy interlayers, the presence of multiple layers of clay-type muddy interlayers sandwiched between relatively hard rock masses can pose significant risks, similar to a "sandwich" structure. We discovered that the sampling site had poor engineering conditions, with 13 layers of muddy interlayers superimposed. Other scholars' sampling sites also had unfavorable engineering conditions, but the occurrence of 13 layers of muddy interlayers superimposed has not been previously reported. Due to certain limitations, researchers have not conducted further experimental studies on clay-type muddy interlayers. These interlayers are located within unstable slopes, have thin thickness and on-site strength testing primarily relies on large-scale in situ tests, which are costly. Obtaining undisturbed samples is also challenging, and conducting a limited number of on-site tests often fails to yield convincing results. In addition, through indoor direct shear-creep tests, it is more convenient to observe how its deformation changes over time under the influence of normal stress, which is the creep behavior.

To sum up, a great deal of research has been carried out on the creep characteristics of weak interlayer and muddy interlayer, which has always been a research hotspot. Because of the difficulty of sampling in the field, the field test is expensive, a small number of experiments are difficult to obtain convincing results and the indoor creep experiment takes a long time, and the creep experimental study of clay interlayer has not been reported. The study of its creep characteristics and long-term strength can fill the gap in the study of muddy interlayer and provide a powerful reference for its research. In this paper, combined with the example of high slope instability project of municipal solid waste incineration power plant in Yuxi City, Yunnan Province, sampling from the accident site, using a stress-controlled direct shear apparatus modified from a strain-controlled direct shear apparatus, the indoor direct shear creep experimental study on clay-type muddy interlayer was carried out. it is expected to provide a reference for the study of the stability of the slope with clay-type muddy interlayer.

2. Methodology

2.1. Materials

The test soil samples were obtained from the instability project of the high slope of the municipal solid waste incineration power plant in Yuxi City, Yunnan Province. During the excavation and support construction, the high slope experienced three times of instability, resulting in the complete failure of most of the supporting structures. After on-site investigation, it is considered that the clay-type muddy interlayer is one of the important factors contributing to the instability of the slope [34]. Field surveys were conducted at the location of the unstable slope, and sampling points were established, as shown in Figure 1. The observed profile at the sampling point has a height of 3.8 m and reveals the presence of 13 layers of mudstone interlayers, denoted as L1 to L13 (as depicted in Figure 1a). These muddy interlayers are continuously distributed laterally across the entire observed profile, exhibiting overall approximate parallelism. The orientation of interlayer L7 is measured as 193° with a dip of 21°, and the spacing between interlayers varies from 3 to 30 cm. The thickness of these muddy interlayers ranges from 1 to 25 mm. Notably, the thickness of muddy interlayers differs between different lateral positions within the same layer and between different layers. For instance, a portion of interlayer L4 has a thickness of 25 mm (as shown in Figure 1b), while another section of the same layer has a thickness of 5 mm (as shown in Figure 1c). Interlayer L9 has an approximate thickness of 2 mm (as depicted in Figure 1d).

2.2. Methods

2.2.1. Preparation of Samples

The collected samples were packaged in bags and transported back. Since the muddy interlayers contained rock particles from the adjacent upper and lower rock layers, it was necessary to remove these particles to avoid any impact on the subsequent creep experiments, as illustrated in Figure 3b. For the indoor preparation of remolded samples for direct shear-creep testing, the sample preparation process was as follows:

(1) The samples were crushed indoors and passed through a sieve with a 2 mm mesh to separate the finer particles below 2 mm, which were used for the remolded samples.
(2) The finer particles were repeatedly mixed and air-dried to achieve the target moisture content. Based on the specified moisture content and dry density, a certain mass of moist soil was weighed and evenly distributed in 3 layers, which were then compacted into sample molds with roughened layer interfaces (as shown in Figure 2a).
(3) The resulting samples were solid cylindrical specimens with a diameter of 61.8 mm and a height of 20 mm. The moisture content was determined to be 20.39% using the

"oven-drying method", and the dry density was measured as 1.93 g/cm^3 using the "ring knife method".

(4) The samples were wrapped with multiple layers of plastic film and tape, then allowed to stand in the HBY-40A Standard Curing Cabinet for 72 h (as depicted in Figure 2b). A total of 10 samples were prepared, including 2 backup samples.

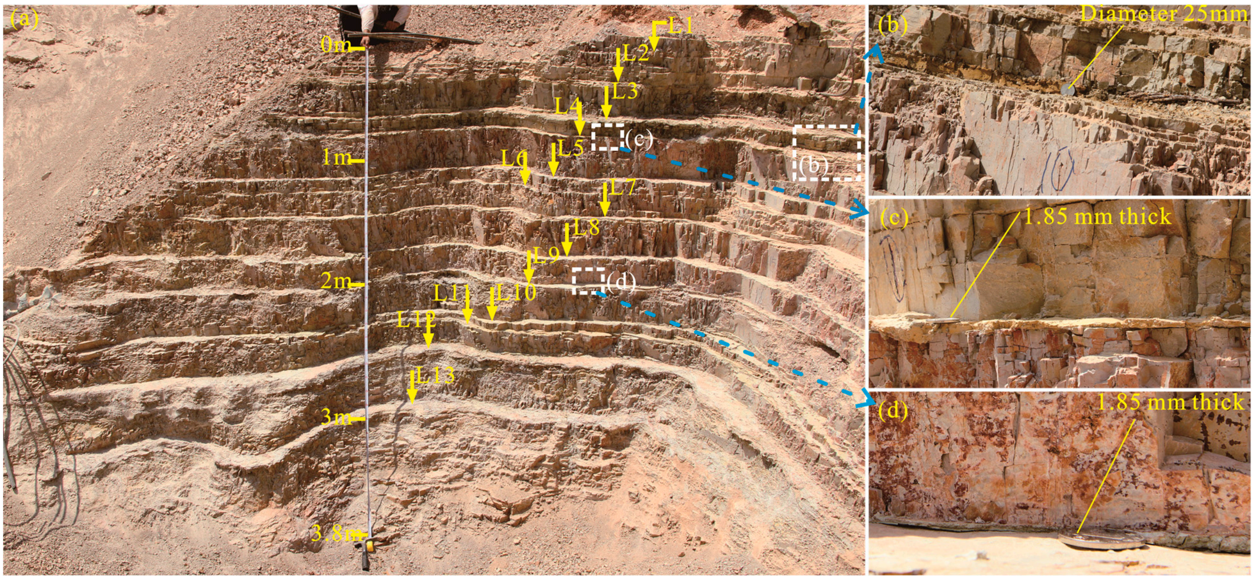

Figure 1. Sampling point distribution of muddy interlayers (**a**) and enlarged views of local positions (**b**–**d**).

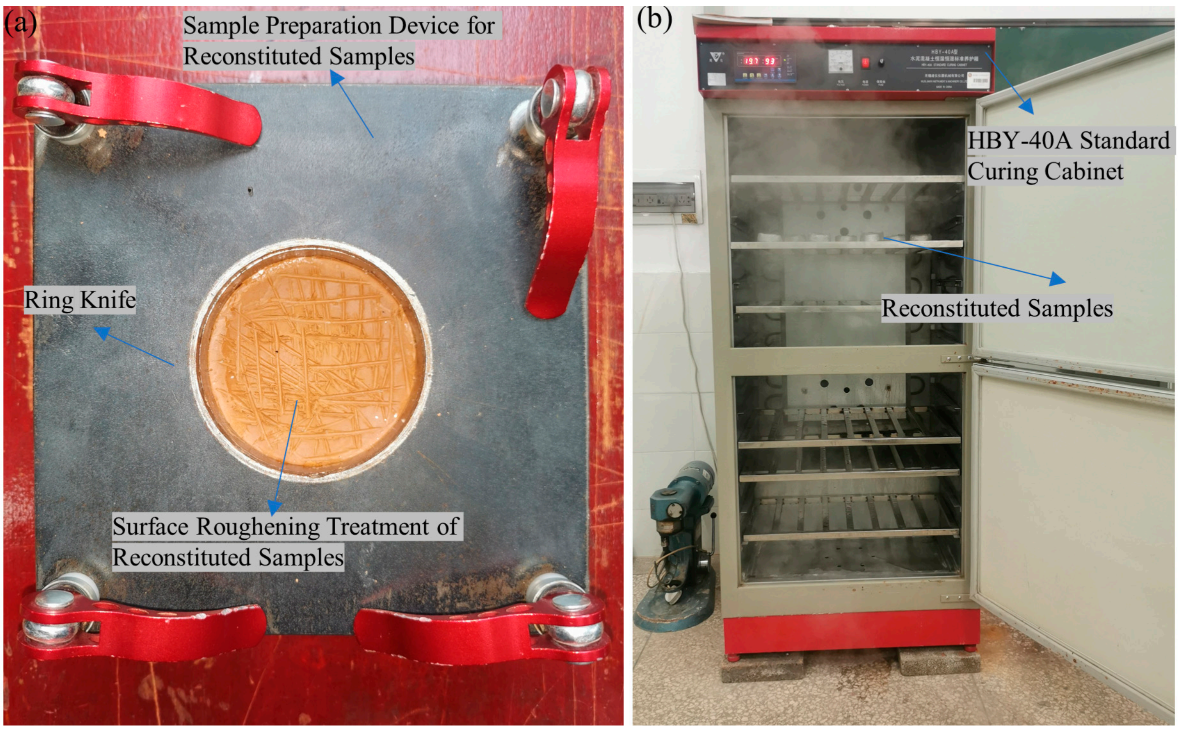

Figure 2. Sample Molder for Remolded Samples (**a**) and HBY-40A Standard Curing Cabinet Illustration (**b**).

Figure 3. Original sample (**a**) and sample treatment diagram of clay-type muddy interlayer (**b**).

2.2.2. Test Equipment

The direct-shear instrument can be divided into two types: strain control type and stress control type. The former is to push the sample to produce displacement at the same speed to measure the corresponding shear stress, while the latter is to apply horizontal shear stress to the specimen to measure the corresponding displacement. The instrument used in this mud interlayer shear-creep test is the stress-controlled direct-shear instrument of the Key Laboratory of Geological Hazard Prevention and Engineering Seismic Resistance of Kunming University of Science and Technology. It is modified from the strain direct-shear instrument, which retains the vertical loading system and measurement system of the original instrument, and adds the shear-loading system and horizontal measurement system by installing fixed pulley and digital display percentage meter. The shear box and measurement system are shown in Figure 4. Shearing box (9 and 10): The shearing box used in the test is composed of upper and lower shearing boxes (water storage boxes). The sample is placed in the shearing box, and a fixed sample shearing surface is formed between the two boxes (the position of the sample is shown in Figure 4), and there is permeable stone on the sample (shown as number 4 in the Figure 4), so that a drainage condition is provided in the shear box. Consolidation pressure is applied vertically, and horizontal shear force is applied along the shear plane, so that the soil sample undergoes direct shear creep deformation along the shear plane. The difficulty of modification control mainly focuses on how to fix the test shear loading system to ensure that the applied shear stress is parallel to the shear plane. Test loading system: The modified stress-type direct-shear instrument test loading system mainly involves two aspects. Among them, the vertical consolidation pressure loading system does not need to be changed, and the loading method of the original strain-type direct-shear instrument can be used as the standard. The horizontal shear loading system is obtained by applying a weight mass, and the vertical gravity is turned into a constant horizontal shear force by setting the pulley. Deformation measurement system (as shown in the numbers 1 and 12 in the figure, the score of the scale is 0.02 mm): This is the biggest difference between the traditional strain-type direct-shear instrument and the modified stress-type direct-shear instrument. The traditional strain-type direct-shear instrument controls the shear displacement value through the constant speed and number of rotations of the motor, and obtains the corresponding shear force under a certain deformation condition through the measuring force ring. The purpose of the stress-type direct-shear instrument is to measure the relationship between the shear deformation of the soil sample and time under a constant shear force. The difficulty of modification control is mainly focused on the transformation of the frame of the original strain-type direct-shear instrument, determining the position and fixing the dial indicator, and obtaining the shear deformation of the soil sample through the reading of the dial indicator.

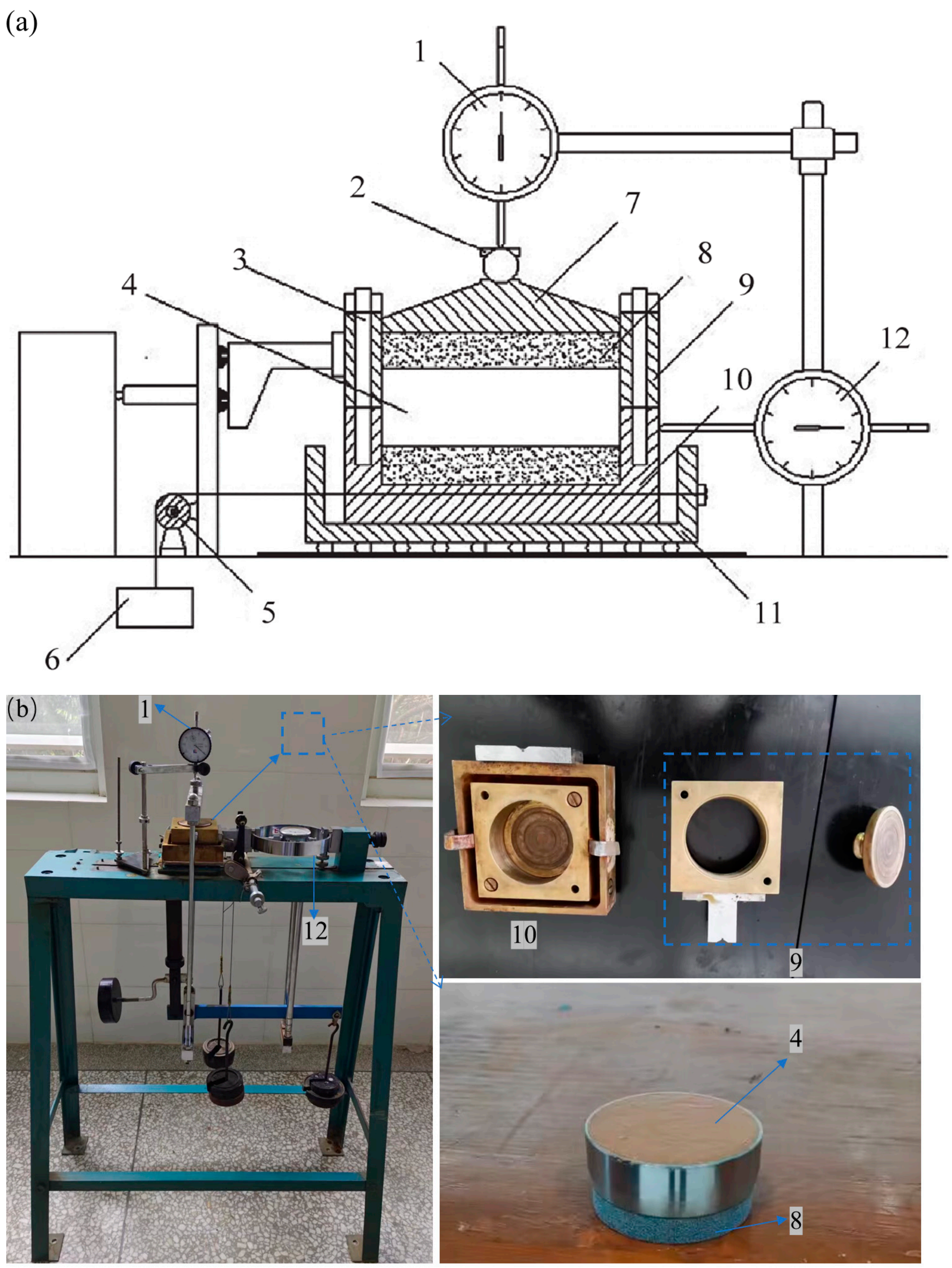

Figure 4. Schematic diagram of stress-controlled direct shear-creep test device (**a**) and instrument diagram (**b**). 1—Vertical displacement scale; 2—Vertical compression frame; 3—Fixing screws; 4—Sample; 5—Crown block; 6—Weight; 7—Normal pressure cover plate; 8—Permeable stone; 9—Box loading; 10—Lower box; 11—Base; 12—Horizontal displacement scale.

2.2.3. Test Procedure and Test Plan

The test is carried out with reference to the industry standard, and the basic steps are as follows:

(1) The fast shear test was carried out on the samples, and at different consolidation pressures (100 kPa, 200 kPa, 300 kPa, 400 kPa), shear at a speed of 0.8 mm/min

(12 rpm) and measure the shear strength (τ_f) of the muddy interlayer under all levels of consolidation pressure.
(2) In the direct shear-creep test, the application of normal stress (100 kPa, 200 kPa, 300 kPa, 400 kPa) is carried out first, followed by consolidation for 24 h. Vertical deformation is then monitored during this period.
(3) Based on the formula $\tau_i = \tau_f / n$ (where n is the loading series, which is taken as 5~7, and τ_f is the shear strength under different consolidation pressures), the shear stress at each level of the direct shear-creep test is determined, combined with the weight of the shear stress weight. The shear stress of each stage is properly adjusted, and creep failure of the rock is ensured when the last level of shear stress is applied, and the loading scheme of this direct shear-creep test is obtained (Table 1).
(4) The instantaneous shear displacement is measured immediately when the first-order shear load is applied, the read shear creep value is tested within a certain time interval, the observation times are encrypted at the early phase of deformation, the number of data-reading decreases after the deformation tends to be basically stable and the shear load of each stage is maintained for 7 days.
(5) When the final level of shear load is applied, if it is found that the shear creep displacement has a tendency to increase rapidly with time, the number of observations should be increased to reflect the final creep failure stage.

Table 1. Indoor direct shear-creep test scheme of muddy interlayer.

Sample Number	Consolidation Pressure/kPa	Shearing Stress/kPa
CD-1	100	7–14–18–21–35–42
CD-2	200	9–18–27–36–45–54–63–72–81–90–99
CD-3	300	10–20–30–40–50–60–70–80–90–100
CD-4	400	12–24–36–48–60–72–84–96–108–120–132–144–156–168

2.2.4. Horizontal Shear Load Loading Method

For the current indoor direct shear-creep test, there are two loading methods to choose from: one is to load separately; the other type is hierarchical loading. The so-called separate loading method refers to a specimen that only bears one level of shear stress from beginning to end, and conducts tests at different shear levels under identical testing equipment and conditions to obtain the entire process curve of specimen creep at different shear levels. Its advantage is that it can largely meet the requirements of creep theory for testing. However, in practical experiments, due to the requirement of using multiple test instruments simultaneously to complete a set of tests with different shear levels, it is also difficult to achieve experimental preparation and implementation. On the one hand, because of the constraints imposed by the testing conditions, it is not possible to provide multiple sets of test equipment for synchronous testing, and on the other hand, due to the limitations of samples, there are many uncontrollable factors in equipment and soil samples, and there is a large consumption of soil samples. In terms of current research on direct shear-creep tests, this loading method is rarely used.

The so-called graded loading mode means that in the entire process of creep test, all levels of horizontal shear stress act on the same sample and are completed with the same test equipment. After applying a certain level of shear force, the soil sample is stable after creep deformation for a period of time, and then the next shear force is applied. The specific creep deformation stability standard can be determined according to the test situation, and the action time of all levels of shear force can also be adjusted in the specific test. In this test method, it is not necessary to consider the interference caused by the differences in the properties of the test equipment and the test soil samples, and the test results obtained are highly reliable. The shortcomings of this loading method are as follows: on the one hand, when all shear levels are applied on the same soil sample, the test cycle will be greatly increased, resulting in soil hardening caused by water evaporation in the soil sample; on the other hand, the influence of each shear level on the test deformation, the application of the first shear level will affect the next shear deformation to a certain extent. Considering the two loading methods, test conditions and the number of samples, it was decided that this series of direct shear-creep tests should be studied by step loading.

2.2.5. Creep Data Processing

The creep test curve obtained by hierarchical loading is shown in Figure 5, and transforming it into separate loading creep curve is a key step in creep analysis. At present, the creep test data with hierarchical loading are mostly processed according to the principle of Boltzmann superposition [35]. Through the study of rheological mechanics for many years, Sun [36] pointed out that geotechnical materials are highly nonlinear, so the creep curve can not be simply superimposed by the creep response of each load.

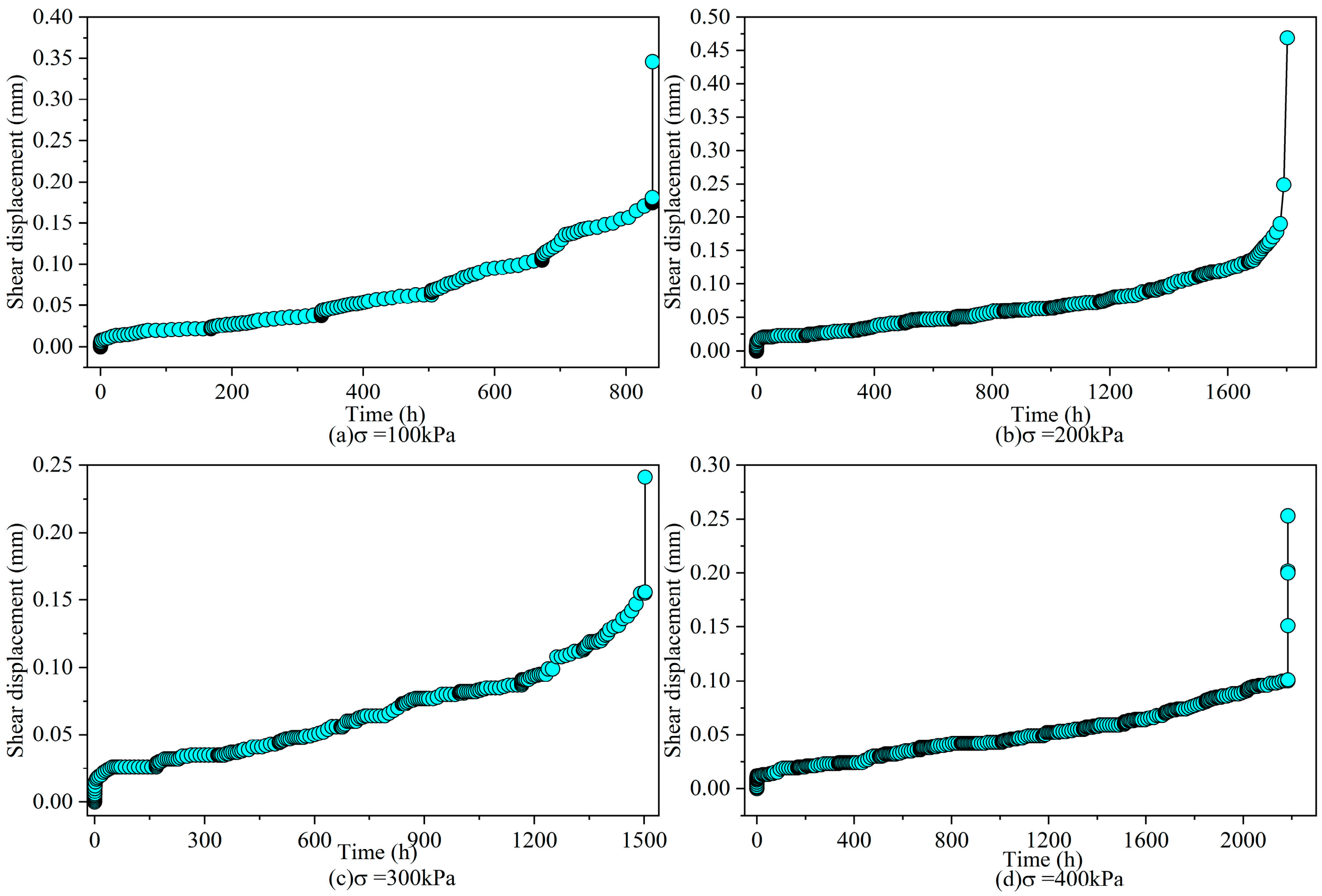

Figure 5. Full creep process curve of graded loading under different normal stresses ((**a**) σ = 100 kPa, (**b**) σ = 200 kPa, (**c**) σ = 300 kPa, (**d**) σ = 400 kPa).

The "Chen's Method" proposed by Chen Zongji in 1964 and developed by his students has been more and more widely used in the study of geotechnical Rheology. The original intention of Chen's method is to use a simple method to derive the stress–strain time relationship from the test results, and apply n steps of load to only one sample to obtain the creep curves of n different samples of the same geotechnical material with n steps of different sizes of load. This is a simple method to solve the nonlinear effect caused by step loading. Its advantage is that by using suitable experimental techniques and methods, the use of graphical methods to establish the superposition relationship of real deformation processes can be applied regardless of whether the aftereffect is linear or nonlinear.

Chen's method can be summed up to answer the following experimental questions [37]: assuming that the step loading of the sample is carried out with a step distance of $\Delta\tau$ as shown in Figure 6a, and the test curve is obtained as shown in Figure 6b, how to infer the creep curve under one-time loading with the load of $\tau_n = \sum_{i=1}^{n} \triangle\tau_i$?

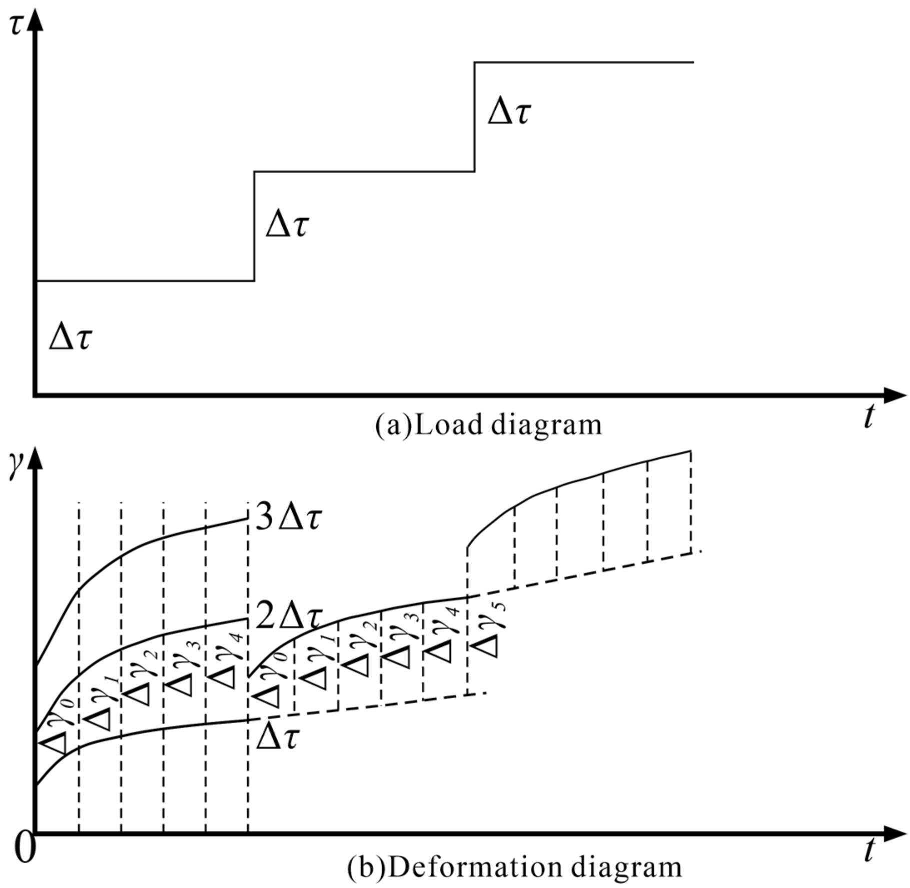

Figure 6. Chen's loading method and creep data processing method ((**a**) Load diagram, (**b**) Deformation diagram).

First, look at the material creep caused by the first level of loading, from time t_0 = 0 to t_0 = t_1, the material is deformed by creep under the constant load t_1 = $\Delta\tau$. If the test is carried out to time t_1 without adding the next level of load $\Delta\tau$, the material deformation will continue to be along the dashed line since the material deformation has already entered into the steady-state creep at this time, so the effect of adding the acting load $\Delta\tau$ to the specimen is that the dashed line occurs additional deformation between the dashed line and the solid line (shown in the shaded line region). It is possible to find, from this additional deformation, the creep value with t_0 as the starting point in time and the creep increment $\Delta\varepsilon(t)$ due to the stress increment $\Delta\tau$ with t_1 as the starting point in time. Therefore, using the first stage of loading as a basis and superimposing the creep increment of the next stage of loading acting with the same continuation time, a one-time loading of $\tau_2 = 2\Delta\tau$ creep curve is obtained. The continuation of the step loading, can be in the previous level of the creep curve on the same treatment, so that a one-time loading of $\tau_n = \sum_{i=1}^{n} \Delta\tau_i$ creep curve can be obtained, such as the dotted area to the left of Figure 6b, so that several creep curves under n different loads can be obtained from one specimen.

When using this method, two points should be paid attention to: (1) when the next stage loading is carried out, the deformation should be carried out after the deformation has entered the steady creep under the previous load; (2) the time interval of step-by-step loading should be equal.

3. Results and Discussion

3.1. Shear Creep Curve of Clay-Type Muddy Interlayer

The creep test curve of this shear-creep test is shown in Figure 7, and the curve shows the values of shear stress at all levels. Through the shear displacement–time curve, it can be seen that the muddy interlayer has obvious creep characteristics, which can be summarized as follows:

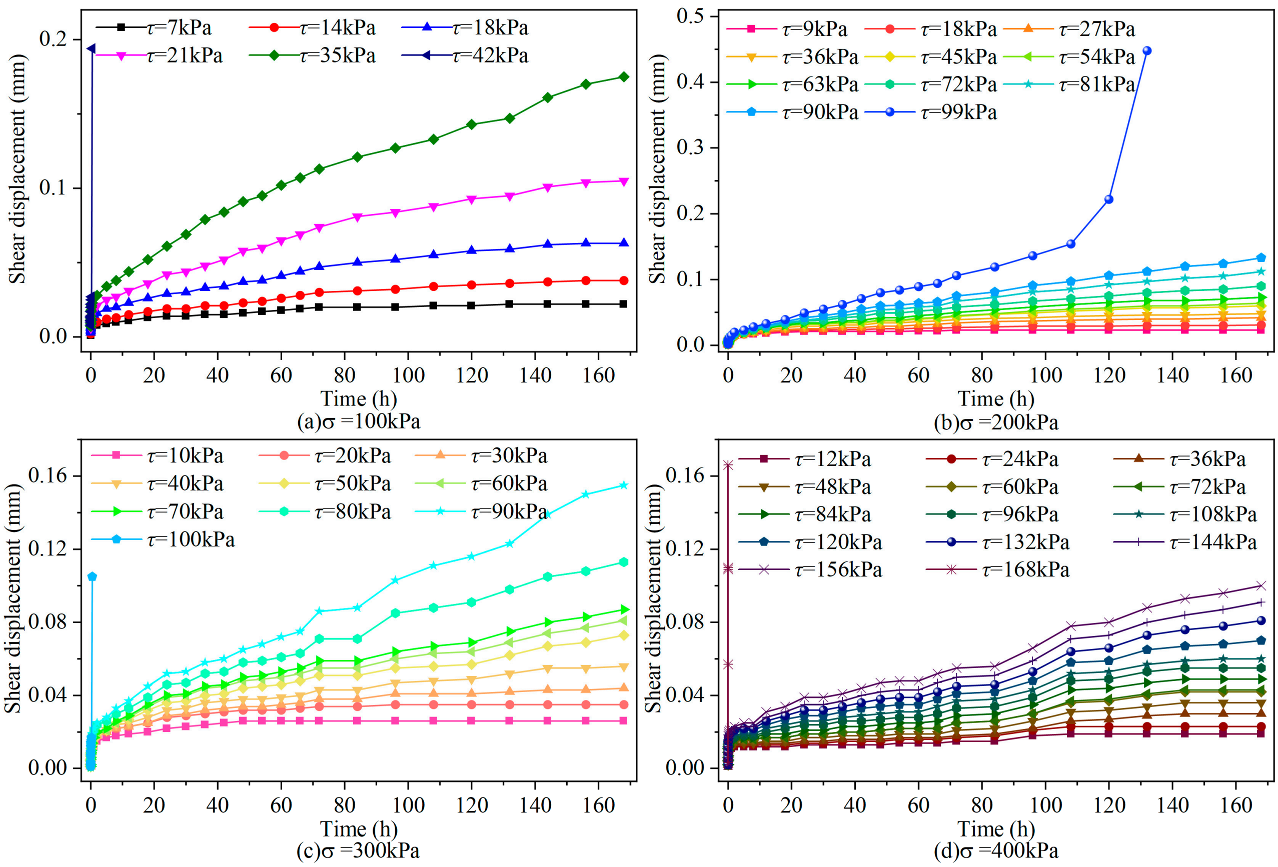

Figure 7. Shear creep curves under different normal stresses ((**a**) σ = 100 kPa, (**b**) σ = 200 kPa, (**c**) σ = 300 kPa, (**d**) σ = 400 kPa).

(1) Under the constant normal stress level, the muddy interlayer sample has transient deformation and initial creep stage after all the levels of shear stress are loaded, and the initial creep stage lasts for a short time. At lower stress levels, the samples exhibited a stable creep stage, characterized by a creep curve that approximates a straight line. When the shear stress is relatively low, the shear displacement basically remains unchanged (the creep rate is approximately 0), and when the shear stress is slightly higher, the shear displacement slowly increases (the creep rate is a small constant value). This suggests that shear stress affects the creep behavior of the mud stratification, a feature noted by some researchers in the shear creep curves of muddy interlayer [38,39]. The accelerated creep stage usually occurs after the application of the last Shear stress, because the shear stress is greater than the critical strength of the impedance capacity of the specimen, during which the shear displacement increases rapidly with time until the specimen is destroyed.

(2) The shear displacement in the initial creep stage increases rapidly with time, while the creep rate decreases rapidly with time, and the creep rate in the stable creep stage increases with the increase in shear stress, indicating that the creep of the muddy interlayer is very strong, and the creep is enhanced with the increase in shear stress.

(3) After the last shear stress is applied, there are three obvious stages of creep (Figure 7b), which shows a typical ductile failure form, while in Figure 7a,c,d, it directly enters the accelerated creep stage and occurs, showing a brittle failure form. It shows that when σ = 200 kPa, the last shear stress is just within the range where three stages of creep can occur, while when σ = 100, 300 and 400 kPa, the last shear stress is outside this range.

(4) According to the curve of test results, it can be seen that the shear failure value of muddy interlayer increases with the increase in normal stress level. This is mainly because the increase in the normal stress level enhances the compaction effect on the interlayer particles and increases the shear friction resistance of the sample, so the shear stress required for shear failure increases accordingly. As shown in Figure 8, even though the vertical compression displacement under σ = 200 kPa is slightly greater than under σ = 300 kPa during the 12 to 408-h period, the difference is quite small, falling within the range of 0.01 to 0.04 mm. In summary, the overall trend in the shear-creep test process shows that the vertical compression displacement of the specimens increases with the rise in normal stress and gradually grows over time.

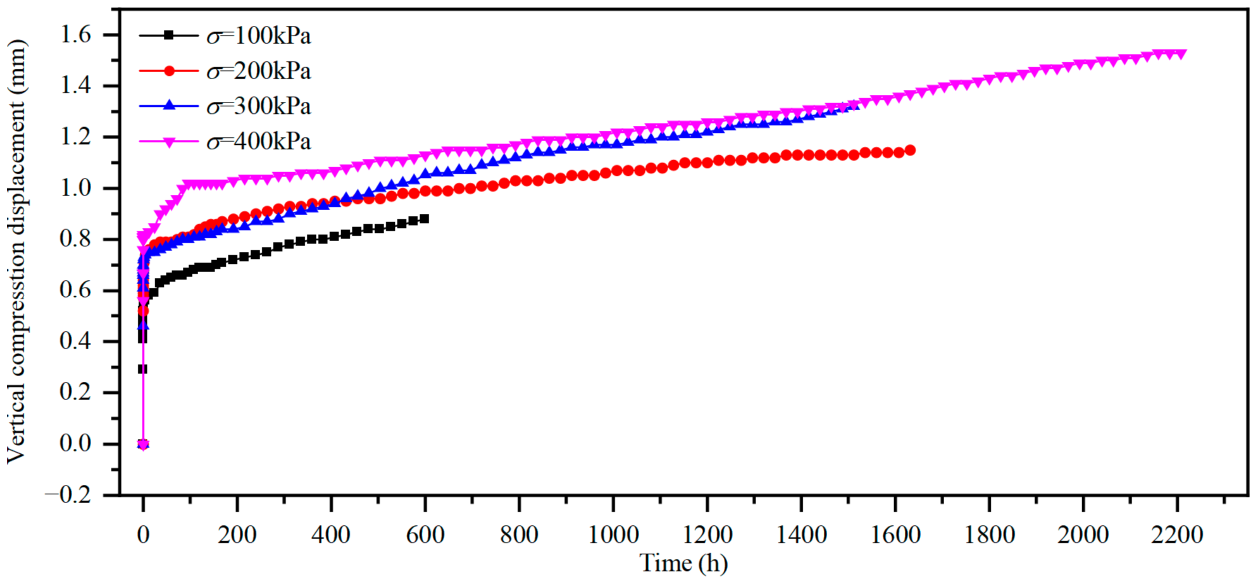

Figure 8. Vertical compression displacement variation diagram under different normal.

3.2. Empirical Formula of Shear Creep

According to the above analysis results of the characteristics of the shear-creep test curve, the following empirical formula was proposed to fit the graded shear-creep test curve:

$$u = u_0 + A(1 - e^{-Bt}) + Ct^n \tag{1}$$

In the formula: u_0 is instantaneous deformation, at constant stress level, A, B, and C are all constant; t is creep time; $A(1 - e^{-Bt})$ characterizes the attenuation creep deformation characteristics of muddy interlayer; and exponent n represents the creep deformation characteristics of muddy interlayer after attenuation creep at different shear stress levels.

In view of the large number of data, Table 2 only gives the fitting parameters of the corresponding shear stress under the normal stress 100 kPa and 200 kPa obtained by empirical formula. The variation range of R^2 is 0.90–0.99, which shows that the proposed empirical formula can well simulate shear creep. The curve is drawn according to the data sorted out by the fitting formula and compared with the experimental data, as shown in Figure 9. From Table 2 and Figure 9, it is evident that when the normal stress is 200 kPa, the empirical formula exhibits less-than-optimal fitting for the application of the final level of shear stress. In this case, the R^2 value is 0.91. However, for all other normal stress levels, the empirical formula shows good fitting results. This suggests that the empirical formula effectively captures the instantaneous deformation, initial creep and steady-state creep of muddy interlayer stratification but falls short in fitting the accelerated creep. Other researchers have also employed different empirical formulas. Lin [38] used a logarithmic function to fit the creep curve when investigating the creep characteristics of mud stratification. Zhou et al. [21] utilized a power function to fit the changes in shear creep deformation over time in muddy layers, achieving good fitting results. Considering the stronger creep characteristics of cohesive mud stratification, these alternative empirical formulas may not be suitable for our study.

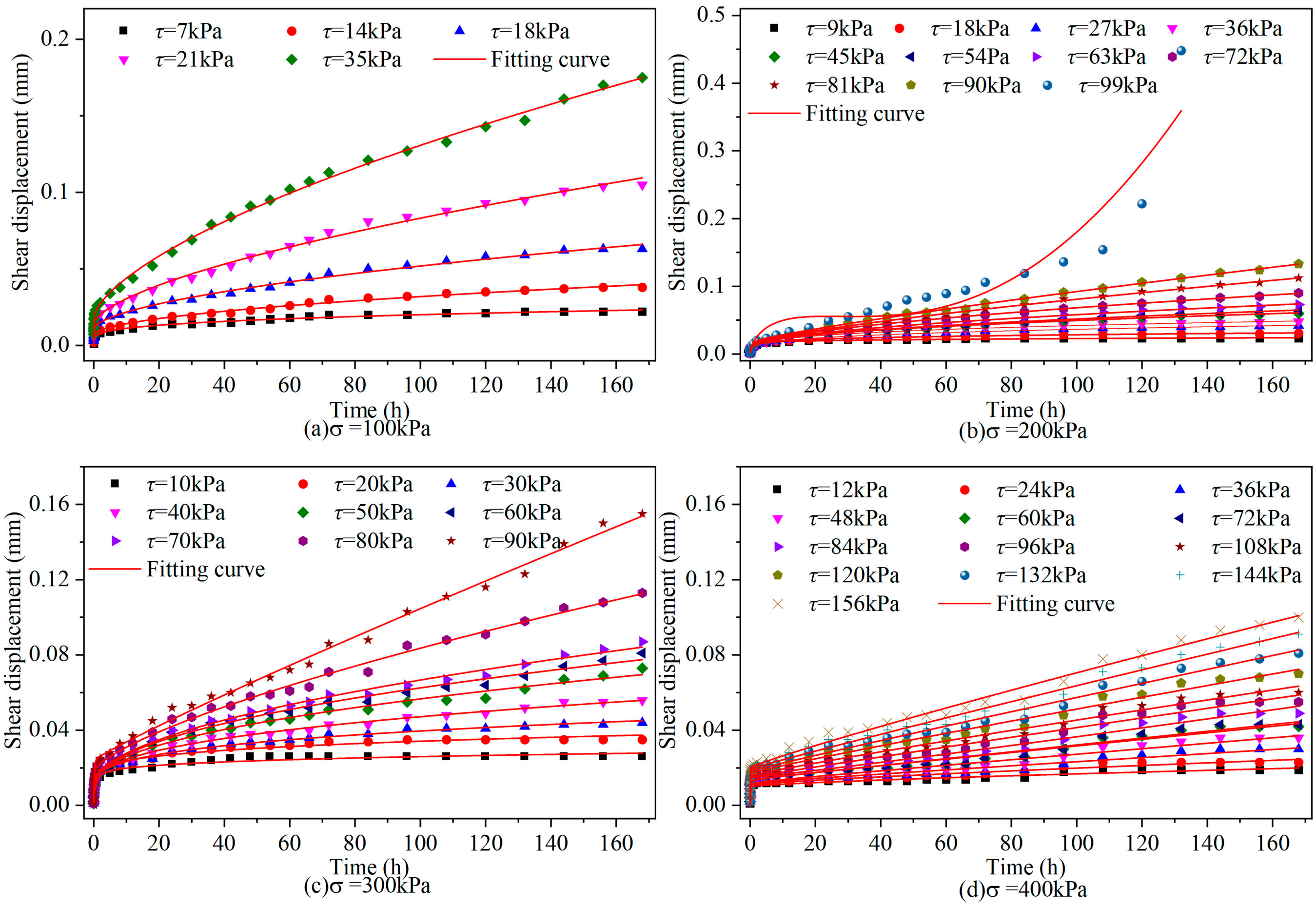

Figure 9. Comparison between the calculated value of empirical formula and the experimental value under different normal stress ((**a**) σ = 100 kPa, (**b**) σ = 200 kPa, (**c**) σ = 300 kPa, (**d**) σ = 400 kPa).

Table 2. Parameter fitting values of empirical formula.

Normal Stress/kPa	Shearing Stress/kPa	u_0/mm	A	B	C	n	R^2
	7	6.5750×10^{-4}	0.0026	17.6874	0.0037	0.3265	0.99
	14	0.0022	0.0043	9.1325	0.0024	0.5170	0.99
100	18	0.0040	0.0066	15.5837	0.0031	0.5658	0.99
	21	0.0066	0.0075	23.4534	0.0039	0.6226	0.99
	35	0.0086	0.0093	28.3479	0.0060	0.6357	0.99

Table 2. *Cont.*

Normal Stress/kPa	Shearing Stress/kPa	u_0/mm	A	B	C	n	R^2
200	9	0.001	0.0099	0.8480	0.0047	0.2019	0.99
	18	0.001	0.0078	0.7980	0.0060	0.2581	0.99
	27	0.001	0.0043	2.1471	0.0067	0.3353	0.99
	36	0.0015	0.0021	1.8468	0.009	0.3153	0.99
	45	0.0042	0.0089	1.4434	0.0032	0.5252	0.99
	54	0.0033	0.0096	1.2755	0.0029	0.5622	0.99
	63	0.0031	0.0077	1.8629	0.0036	0.5597	0.99
	72	0.0040	0.0076	2.4687	0.0034	0.6133	0.99
	81	0.0041	0.0101	1.9092	0.0022	0.7456	0.99
	90	0.0043	0.0130	1.2354	0.0016	0.8343	0.99
	99	0.004	−52.2502	0.0016	0.0969	0.9556	0.91

3.3. Variation Law of Shear Creep Rate

From Figure 7, the corresponding slopes of creep curves at different shear stress levels are calculated, and the average and steady-state shear creep rates of muddy interlayers under different stress states are obtained. As there are many data results, the creep results of normal stress 100 kPa and 400 kPa are listed in Table 3.

Table 3. Analysis of shear creep rate.

Normal Stress/kPa	Shearing Stress/kPa	Average Creep Rate/(10^{-2} mm·h^{-1})	Steady Creep Rate (10^{-2} mm·h^{-1})
100	7	0.0125	0.0084
	14	0.0214	0.0168
	18	0.0351	0.0287
	21	0.0583	0.0509
	35	0.0988	0.0892
400	12	0.0107	0.006
	24	0.0125	0.0077
	36	0.0167	0.0119
	48	0.0202	0.0155
	60	0.0238	0.0179
	72	0.0244	0.0185
	84	0.0268	0.0214
	96	0.0303	0.0250
	108	0.0333	0.0274
	120	0.0393	0.0328
	132	0.0452	0.0387
	144	0.0512	0.0441
	156	0.06	0.0488

It can be seen from Table 3 that under the constant normal stress level, the shear creep of each sample increases with the increase in the shear stress level, and the average creep rate of the muddy sandwich specimen is basically one- to three-times that of the stable creep rate. It shows that the initial attenuation creep stage of the specimen under all levels of stress has small deformation, short duration and long stable creep duration, and the creep of muddy interlayer is very significant. The stable creep rate basically remains constant at the constant stress level, and the steady creep rate at the lower shear stress level is a constant greater than 0, indicating that the muddy interlayer produces significant creep deformation at the lower stress level.

According to the analysis results of Table 3, the curves of the relationship between average creep rate and shear stress under different normal stress levels were fitted. At the same normal stress level, the relationship between average creep rate and shear stress can be expressed as an exponential function:

$$u_a = ae^{b\tau} \tag{2}$$

In the formula: a and b are the material parameters of the muddy interlayer, as shown in Table 4. The curve of the relationship between average creep rate and shear stress is shown in Figure 10a. The fitting curve in the graph closely aligns with the data points, demonstrating a strong agreement. The range of the correlation coefficient R^2 for the fitting parameters varies from 0.91 to 0.99, indicating a high level of fitting performance. The average creep rate at different normal stress levels increases exponentially with the increase in shear stress.

Table 4. Fitting parameters of average creep rate.

Normal Stress/kPa	a	b	R^2
100	0.0125	0.06	0.91
200	0.0126	0.0199	0.99
300	0.0133	0.0208	0.97
400	0.0109	0.0108	0.99

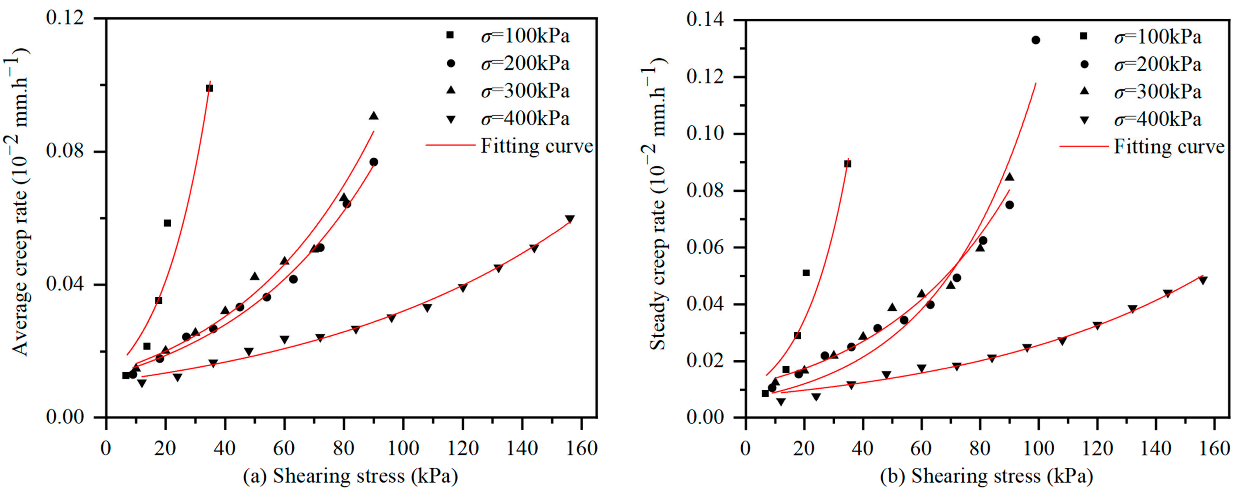

Figure 10. Relationship between average shear creep rate (**a**) or steady shear creep rate (**b**) and shear stress of muddy interlayer.

As the main part of the shear creep of muddy interlayer, the stable creep stage lasts a long time and has a significant impact on the stability of the slope. Similarly, according to the analysis results of Table 3, the relationship curve between stable creep rate and shear stress level under different normal stress level can be fitted. At the same normal stress level, the relationship between stable creep rate and shear stress of muddy interlayer is an exponential function.

$$u_s = ce^{d\tau} \tag{3}$$

In the formula: c and d are the material parameters of the muddy interlayer, as shown in Table 5. The curve of the relationship between stable creep rate and shear stress is shown in Figure 10b. The fitting curve in the graph closely aligns with the data points, demonstrating a strong fit. The range of the correlation coefficient R^2 for the fitting parameters varies from 0.91 to 0.99, indicating a high level of fitting performance. The steady creep rate at different normal stress levels increases exponentially with the increase in shear stress.

Table 5. Fitting parameters of stable creep rate.

Normal Stress/kPa	c	d	R^2
100	0.0096	0.0644	0.91
200	0.0068	0.0288	0.93
300	0.0133	0.0218	0.97
400	0.0077	0.0120	0.99

3.4. Study on Long-Term Strength of Muddy Interlayer

The long-term strength of the muddy interlayer is the boundary value that distinguishes the attenuation creep from the nonattenuation creep, and researching the long-term strength of the muddy interlayer can provide valuable references for the stability analysis and evolution prediction of landslides. Rock and soil, in a given period of time, produce damage to the impedance ability that is known as its long-term strength $\tau(t)$, and its long-term strength limit τ_∞, that is, the rock and soil in the long-term load under the action of the impedance ability of the critical strength value, that is, the rock and soil strength with the extension of the action of the time and the lowest value of the reduction. At the same moment, shear creep deformation increases with the increase in shear load; when the shear load is below the long-term strength, the sample undergoes attenuation creep, and the specimen is not damaged; when the shear load surpasses the long-term strength, the sample exhibits steady-state creep and accelerated creep, which finally leads to the destruction of the specimen with the development of time.

Usually, the long-term strength of soil creep can be determined by the following two methods [40,41]: (1) To draw the stress–deformation curve based on the test results of cascade loading in logarithmic coordinates. It is found that the stress with obvious inflection point on the curve in logarithmic coordinates is taken as the limit value of long-term strength τ_∞. (2) The long-term strength limit is the boundary value that distinguishes attenuated creep from nonattenuated creep, so the curve between stress and strain rate under this stress can be drawn, and the intersection of the curve and stress axis is the long-term strength limit value τ_∞.

The isochronous cluster curve of the muddy interlayer under different normal stress is shown in Figure 11, and the inflection point of the cluster curve is not obvious. Therefore, according to the method of Liu et al. and Wang et al. [42,43], it is challenging to precisely determine the long-term strength of muddy interlayer. In view of this, according to the definition of long-term ultimate strength, the long-term strength of muddy interlayer is determined by the following methods: take normal stress 100 kPa as an example, as shown in Figure 7a, the specimen shows attenuated creep at a shear stress of 35 kPa, and nonattenuated creep when shear stress is 42 kPa, indicating that long-term strength limit τ_∞ is between 35~42 kPa, and their average value is taken as long-term strength limit, namely 38.5 kPa. As shown in Figure 12, the long-term cohesion c_∞ is 4.75 kPa and the long-term internal friction angle φ_∞ is 20.4°.

Previous researchers have classified weak interlayers based on their material composition, microstructure and origins, generally categorizing them into four types: primary soft rock, interbedded shear zones (fault zones), muddy interlayer and sliding zones [44]. Zhu et al. [45] conducted a study on the long-term strength evolution of weak interlayers in Permian carbonaceous shales in the southwestern Karst mountain area. They investigated three evolutionary stages, including primary soft rock, interbedded shear zones and sliding zones. During the evolutionary process, long-term strength decreases, with the long-term cohesion (c_∞) of the final evolutionary stage being 0.096 MPa and the angle of internal friction (φ_∞) being 29.6°. Cheng et al. [46] performed indoor direct shear-creep tests on weak interlayers in red sedimentary rocks. For sample 1, they determined a long-term cohesion (c_∞) of 18 kPa and an angle of internal friction (φ_∞) of 17.8°. In comparison to previous studies on no-clay-type muddy interlayer, the long-term strength of clay-type muddy interlayer is notably low and exhibits significant creep characteristics.

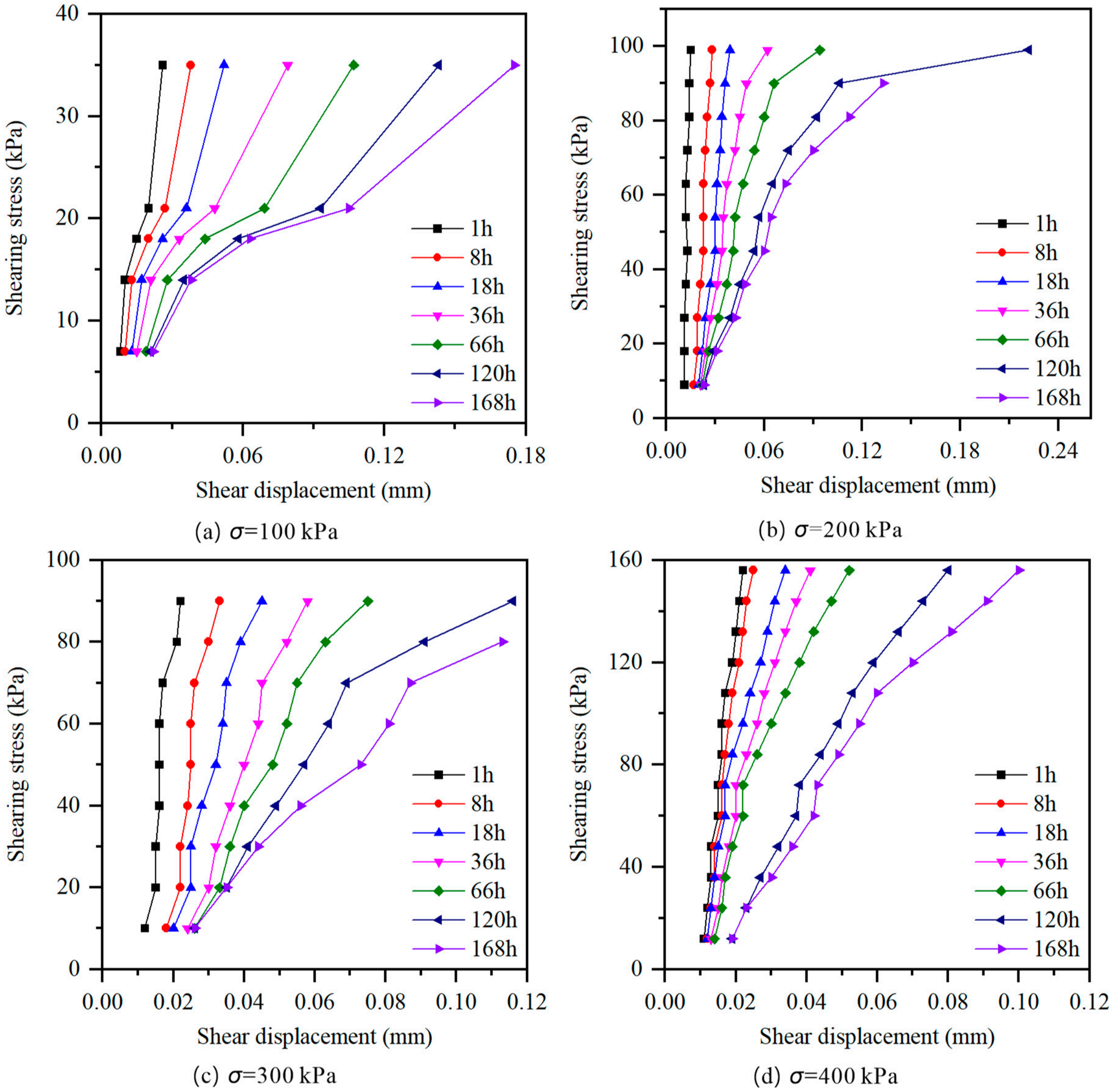

Figure 11. Isochronous cluster curves of specimens under different normal stresses ((**a**) σ = 100 kPa, (**b**) σ = 200 kPa, (**c**) σ = 300 kPa, (**d**) σ = 400 kPa).

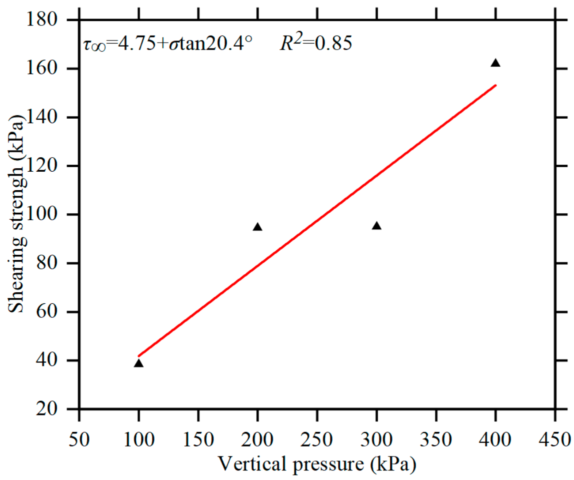

Figure 12. The relation curve between specimen τ_∞ and normal stress σ.

4. Conclusions

Investigations on clay-type muddy interlayer were conducted through laboratory direct shear-creep tests using the convenient staged loading method. Experimental data were recorded, and the complete creep curve was obtained. The 'Chen method' was subsequently employed to transform it into separate loading creep curves. Analysis of the shear–displacement curve was carried out to study the creep characteristics of the muddy interlayer. Based on the analysis of the creep-test curve and the use of empirical formulas to fit several creep stages, the study then explored the relationships between average and stable creep rates and shear stress. A method for determining the long-term strength limit was proposed. The main results obtained are as follows:

(1) The shear creep deformation of the clay-type muddy interlayer is obvious. At the same normal stress level, the specimen has instantaneous deformation, initial creep and stable creep at the lower shear stress level. There are two cases at the level of rupture shear stress: the creep curve includes three stages of typical initial creep, stable creep and accelerated creep failure or directly enters the accelerated creep stage until the specimen failure. The empirical formula of shear creep proposed, $u = u_0 + A\,[1 - e^{(-Bt)}] + Ct^n$, can well reflect the instantaneous deformation, initial creep and stable creep of shearing interlayer, but the fitting effect of accelerated creep is not good. The coefficient of determination (R^2) for the fitting of the shear creep empirical formulas is consistently above 0.9.

(2) Under the constant normal stress level, the shear creep increases with the increase in the shear stress level, while at the same shear stress level, the shear creep decreases with the increase in the normal stress level. At all levels of stress, the initial attenuated creep stage of the specimen has smaller deformation, shorter duration, longer stable creep duration and the steady creep rate at lower shear stress level is a constant greater than 0, which shows that the creep of the clay-type muddy interlayer is very strong.

(3) Under the same normal stress level, the average and steady creep rate of the clay-type muddy interlayer can be characterized by the exponential function of $\dot{u} = me^{n\tau}$, and the average creep rate of the clay-type muddy interlayer specimens is generally one- to three-times the stable creep rate.

(4) In comparison to previous studies on no-clay-type muddy interlayer, the long-term strength of clay-type muddy interlayer is notably low. A method was proposed to determine long-term shear strength indicators based on the long-term strength limit. By curve fitting, φ_∞ was determined to be 20.4° and c_∞ was 4.75 kPa. The relationship between the shear strength limit (τ_∞) and normal stress (σ) was formulated as $\tau_\infty = 4.75 + \sigma \tan 20.4°$.

Author Contributions: Conceptualization, P.G. and J.Z.; methodology, W.L., Z.W. and J.Z.; software, P.G. and J.Z.; validation, P.G. and F.L.; formal analysis, P.G.; investigation, P.G., W.L., Z.W., J.C. and J.Z.; resources, W.L. and Z.W.; writing—original draft preparation, P.G. and J.Z.; writing—review and editing, P.G., W.L., Z.W. and J.Z.; visualization, P.G. and J.Z.; supervision, J.C. and J.Z.; project administration, W.L., Z.W. and J.Z.; funding acquisition, J.Z. All authors have read and agreed to the published version of the manuscript.

Funding: This research was funded by the National Nature Science Foundation of China, grant number 41807258, Application Code: D0705, Project Category: Youth Science Fund Project, Leader: Zhang Jiaming.

Institutional Review Board Statement: Not applicable.

Informed Consent Statement: Not applicable.

Data Availability Statement: Data are containedwithin the article.

Conflicts of Interest: Author Wenlian Liu and Zhiqiang Wang were employed by the company China Nonferrous Metals Industry Kunming Survey and Design Institute Co. The remaining authors declare that the research was conducted in the absence of any commercial or financial relationships that could be construed as a potential conflict of interest.

References

1. Wang, X.; Liu, W.; Nai, L. Fabric types and microstructure of clay partings. *J. Jilin Univ.* **1983**, *28*, 73–82+133–134. (In Chinese with English Abstract). Available online: https://kns.cnki.net/kcms2/article/abstract?v=3uoqIhG8C44YLTlOAiTRKth5mPLKqXjbyzE23kHsboOHJaCyyuzqfd5NMADEpWqjvV9j9W02ZbUZpzyGJ2sxitHkBB_S5_Hv&uniplatform=NZKPT (accessed on 3 May 1983).
2. Xiao, S. The creep model of intercalated clay layers and change of their microstructure during creep. *Chin. J. Rock Mech. Eng.* **1987**, *6*, 113–124. (In Chinese with English Abstract). Available online: https://kns.cnki.net/kcms2/article/abstract?v=3uoqIhG8C44YLTlOAiTRKqd0WnNPv0wTDjtDUwHroNx-oi0hV0oZNa9sRf3vquNzlU_KZjhqW-migptnk8iR9jy-KLfMypSu&uniplatform=NZKPT (accessed on 19 June 1985).
3. Yi, J.; Sun, J.; Xian, J. The research of the microscopic characteristics of the argillation intercalation'evolution process in southwest red bed area. *Sci. Technol. Eng.* **2016**, *16*, 123–126+145. (In Chinese with English Abstract). Available online: https://kns.cnki.net/kcms2/article/abstract?v=3uoqIhG8C44YLTlOAiTRKibYlV5Vjs7ijP0rjQD-AVm8oHBO0FTadp8CR-pyvgMkjPir9eSjoyAmDnu-4n1xKmMcNHt9PJ0W&uniplatform=NZKPT (accessed on 29 December 2015).
4. Li, A.; Deng, H.; Zhang, H.; Liu, H.; Jiang, M. The Shear-Creep Behavior of the Weak Interlayer Mudstone in a Red-Bed Soft Rock in Acidic Environments and Its Modeling with an Improved Burgers Model. *Mech. Time-Depend. Mater.* **2023**, *27*, 1–18. [CrossRef]
5. Wang, Z.; Zhang, L.; He, J. Influence of mudded intercalation on slope stability and its controlling. *J. Qingdao Inst. Archit. Eng.* **2004**, *25*, 1–4+11, (In Chinese with English Abstract). Available online: https://kns.cnki.net/kcms2/article/abstract?v=3uoqIhG8C44YLTlOAiTRKgchrJ08w1e7eeyE9jLkqq_srXG7yXobLTtm_mWMMExX7X70tIjkTM9Q_66QwdvnjhFWRIZr7Mkv&uniplatform=NZKPT (accessed on 18 October 2004).
6. Gong, J.; Jing, F.; Zhang, K.; Zhou, B. Influence on slope stability of physical-mechanical property of clayer thin interlayer in red sandstone. *J. Chongqing Jiaotong Univ. (Nat. Sci.)* **2010**, *29*, 220–223. (In Chinese with English Abstract). Available online: https://kns.cnki.net/kcms2/article/abstract?v=3uoqIhG8C44YLTlOAiTRKgchrJ08w1e7_IFawAif0mwOIHgfNHDSrp6on16RFgZ-eQNRiAYNODSALsT0DfgFHqJTSx2VPAyn&uniplatform=NZKPT (accessed on 28 September 2009).
7. Bai, Y.; Wang, Y.; Ge, H.; Ni, H. Formation evolution and genetic mechanism of baisheng landslide in the deep-incised valley of jinsha river. *J. Jilin Univ. (Earth Sci. Ed.)* **2019**, *49*, 1680–1688. (In Chinese with English Abstract). [CrossRef]
8. Jaiswal, A.; Verma, A.K.; Singh, T.N. Evaluation of Slope Stability through Rock Mass Classification and Kinematic Analysis of Some Major Slopes along NH-1A from Ramban to Banihal, North Western Himalayas. *J. Rock Mech. Geotech. Eng.* **2023**, *in press*. [CrossRef]
9. Dahal, R.K.; Hasegawa, S.; Yamanaka, M.; Dhakal, S.; Bhandary, N.P.; Yatabe, R. Comparative analysis of contributing parameters for rainfall-triggered landslides in the Lesser Himalaya of Nepal. *Environ. Geol.* **2008**, *58*, 567–586. [CrossRef]
10. Tan, X.; Ren, Y.; Li, T.; Zhou, S.; Zhang, J.; Zhou, S. In-Situ Direct Shear Test and Numerical Simulation of Slate Structural Planes with Thick Muddy Interlayer along Bedding Slope. *Int. J. Rock Mech. Min. Sci.* **2021**, *143*, 104791. [CrossRef]
11. Han, G.; Zhang, C.; Zhou, H.; Zhang, C.; Gao, Y.; Singh, H.K. A New Predictive Method for the Shear Strength of Interlayer Shear Weakness Zone at Field Scales. *Eng. Geol.* **2021**, *295*, 106449. [CrossRef]
12. Xu, G. Study of the Argillaceous Interlayer at the Dam Site of the Qikou Key Water Project. *Yellow River* **1994**, *46*, 33–35+62. (In Chinese with English Abstract). Available online: https://kns.cnki.net/kcms2/article/abstract?v=3uoqIhG8C44YLTlOAiTRKjkpgKvIT9NkGsvn6cq9Bo1u7azdm2rZne3hzgD4OFVAFIezcmEJCM1HmqDlDvhSTYRaNOv0m7TC&uniplatform=NZKPT (accessed on 1 November 2023).
13. Qi, S.; Shi, S.; Tan, J. Engineering Geological Research on the Siltized Intercalation of Flood-relief Stilling Pool of Xiaolangdi Project. *J. Yellow River Conserv. Tech. Inst.* **1999**, *11*, 4–8. (In Chinese) [CrossRef]
14. Chen, R. Study on Geological characteristics and Countermeasures of muddy interlayer in Foundation. *Resour. Environ. Eng.* **2008**, *22*, 55–58, (In Chinese with English Abstract) [CrossRef]
15. Hu, Q.; He, S.; Ye, T.; He, L.; Cai, Q. Microsfabric parameters's quantitative method of the mudded weak interlayer. *Chin. J. Geol. Hazard Control* **2017**, *28*, 137–146. (In Chinese with English Abstract) [CrossRef]
16. Qu, Y.; Shan, S.; Xu, X.; Shi, M. Occurrence of argillitization interbeds and the trend of its changes in a certain construction project. *Chin. J. Geol.* **1977**, *20*, 363–371. (In Chinese with English Abstract) [CrossRef]
17. Liu, H. Preliminary Study on the Distribution of Clay Interactions at the Longmen Dam Site. *Yellow River* **1987**, *39*, 59–64. (In Chinese with English Abstract). Available online: https://kns.cnki.net/kcms2/article/abstract?v=Mw9W0jY1lXC8YClYcDjS7Ghcj3PHBxLrBuBqo-xbp5BdRmTY_pw5zkEcWrnBSCWPs_VqZU5uh7OYy8NOufoRLv6xENMHTwI3TSIbCTVS6dXRRqxZn3LoQ4H1azXqenTzuBSuwJNxjLo=&uniplatform=NZKPT&language=CHS (accessed on 1 November 2023).
18. Zhang, J. Advances in the Engineering Geological Properties of Weak Intercalation. *J. Geol. Hazards Environ. Preserv.* **2020**, *31*, 104–112. [CrossRef]
19. Zhao, D.; Xia, Y.; Zhang, C.; Tang, C.; Zhou, H.; Liu, N.; Singh, H.K.; Zhao, Z.; Chen, J.; Mu, C. Failure Modes and Excavation Stability of Large-Scale Columnar Jointed Rock Masses Containing Interlayer Shear Weakness Zones. *Int. J. Rock Mech. Min. Sci.* **2022**, *159*, 105222. [CrossRef]

20. Han, G.; Zhang, C.; Singh, H.K.; Huang, S.; Zhou, H.; Gao, Y. A Comprehensive Investigation of Engineering Geological Characteristics of Interlayer Shear Weakness Zones Embedded within Baihetan Hydropower Station. *Tunn. Undergr. Space Technol.* **2023**, *132*, 104891. [CrossRef]
21. Zhou, X.; Sun, J.; Liu, G.; Li, Z.; Yi, B. Experimental study of direct shear creep on long-term strength of slope rock mass mudded intercalation based on power function. *Saf. Environ. Eng.* **2018**, *25*, 6–11. (In Chinese with English Abstract). [CrossRef]
22. Han, G.; Hou, J.; Zhou, H.; Zhang, C.; Gao, Y.; Yang, L.; Chen, P. Shear creep experimental study on constitutive model of interlayer shear weakness zones. *Chin. J. Rock Mech. Eng.* **2021**, *40*, 958–971. (In Chinese with English Abstract). [CrossRef]
23. Tang, L.; Zhao, Y.; Liao, J.; Liu, Q. Creep Experimental Study of Rocks Containing Weak Interlayer Under Multilevel Loading and Unloading Cycles. *Front. Earth Sci.* **2020**, *8*, 519461. [CrossRef]
24. Zuo, J.; Wang, Z.; Zhou, H.; Pei, J.; Liu, J. Failure behavior of a rock-coal-rock combined body with a weak coal interlayer. *Int. J. Min. Sci. Technol.* **2013**, *23*, 907–912. [CrossRef]
25. Chen, Q.; Zhang, C.; Yang, C.; Ma, C.; Pan, Z.; Daemen, J.J.K. Strength and Deformation of Tailings with Fine-Grained Interlayers. *Eng. Geol.* **2019**, *256*, 110–120. [CrossRef]
26. Ren, M.; Zhang, Q.; Chen, S.; Zhang, L.; Jiao, Y.; Xiang, W. Experimental Study on Mechanical Properties of Anchored Rock-Like Material with Weak Interlayer Under Uniaxial Compression. *Geotech. Geol. Eng.* **2020**, *38*, 4545–4556. [CrossRef]
27. Miao, H.; Wang, G. Effects of Clay Content on the Shear Behaviors of Sliding Zone Soil Originating from Muddy Interlayers in the Three Gorges Reservoir, China. *Eng. Geol.* **2021**, *294*, 106380. [CrossRef]
28. Chen, Z.; Jia, C.; Lei, M. Experimental investigation on shear creep properties of natural structural plane. *J. Railw. Sci. Eng.* **2021**, *18*, 1817–1827. (In Chinese with English Abstract). [CrossRef]
29. Chen, X.; Li, J.; Chai, J.; Bai, J. Shear creep characteristics and constitutive model for interlayer shear belt of high abutment slopes. *Chin. J. Geotech. Eng.* **2013**, *35*, 1675–1682. (In Chinese with English Abstract). Available online: https://kns.cnki.net/kcms2/article/abstract?v=3uoqIhG8C44YLTlOAiTRKgchrJ08w1e7xAZywCwkEELDQ9z-af4ggJVnwfPVCpvc2o4dnpFptal-YctWiVg3wPh-17q0Gkh9&uniplatform=NZKPT (accessed on 10 April 2013).
30. Namazi, E.; Mohamad, H.; Jorat, M.E.; Hajihassani, M. Investigation on the Effects of Twin Tunnel Excavations Beneath a Road Underpass. *Electron. J. Geotech. Eng.* **2011**, *16*, 441–450.
31. Jusoh, S.N.; Mohamad, H.; Marto, A.; Mohd Yunus, N.Z.; Kasim, F. Segment's joint in precast tunnel lining design. *J. Teknol.* **2015**, *77*, 91–98. [CrossRef]
32. Han, Y.; Liu, X.; Li, D.; Tu, Y.; Deng, Z.; Liu, D.; Wu, X. Model Test on the Bearing Behaviors of the Tunnel-Type Anchorage in Soft Rock with Underlying Weak Interlayers. *Bull. Eng. Geol. Environ.* **2020**, *79*, 1023–1040. [CrossRef]
33. Ma, C.; Zhan, H.; Zhang, T.; Yao, W. Investigation on Shear Behavior of Soft Interlayers by Ring Shear Tests. *Eng. Geol.* **2019**, *254*, 34–42. (In Chinese) [CrossRef]
34. Zhao, Z.; Liu, W.; Wang, Z. *Investigation Report on Side (Slip) Slope Management Project for Yuxi City Domestic Waste Incineration Power Generation Project*; Kunming Prospecting Design Institute of China Nonferrous Metals Industry Co., Ltd.: Kunming, China, 2019. (In Chinese)
35. Zhang, X.; Wang, C.; Zhang, S. Comparative analysis of soft clay creep data processing method. *J. Jilin Univ. (Earth Sci. Ed.)* **2010**, *40*, 1401–1408. (In Chinese with English Abstract). [CrossRef]
36. Sun, J. Rock rheological mechanics and its advance in engineering applications. *Chin. J. Rock Mech. Eng.* **2007**, *26*, 1081–1106. (In Chinese with English Abstract). Available online: https://kns.cnki.net/kcms2/article/abstract?v=3uoqIhG8C44YLTlOAiTRKgchrJ08w1e7aLpFYbsPrqHSoo-GpMay_95KlUErlN6X5ExWvotyiXn0sx1czE6yO2tZUOKhUXEw&uniplatform=NZKPT (accessed on 15 January 2007).
37. Liu, X. *Introduction to Rock Rheology*, 1st ed.; Geological Publishing House: Beijing, China, 1994; pp. 139–143.
38. Lin, W. Study on the Selection of Strength of Mudrock Intercalations in the Gezhouba Dam Foundation. *J. Hydraul. Eng.* **1982**, *27*, 68–72. (In Chinese with English Abstract) [CrossRef]
39. Liu, Q.; Zhu, Z. Shear characteristics of siltized intercalation in red sandstone at different water contents. *J. Shenyang Univ. Technol.* **2012**, *34*, 220–223+235. (In Chinese with English Abstract)
40. Yuan, J.; Wang, X.; Dong, J.; Yang, X. Research on the strength and deformation of shanghai clayey soils under k 0 consolidation condition. *Dam Obs. Geotech. Tests* **1999**, *23*, 31–34. (In Chinese with English Abstract). Available online: https://kns.cnki.net/kcms2/article/abstract?v=3uoqIhG8C44YLTlOAiTRKjkpgKvIT9Nkm5tS6uBYqSGn_m8p0YXqh5ZmQgYdNxs3OXuKRjVjfq9LvDrLi7x44ioPT1gsDaWn&uniplatform=NZKPT (accessed on 12 April 1998).
41. Sun, D.; Yao, Y.; Yin, Z. Elasto-plastic model for soil with initially stress-induced anisotropy. *Rock Soil Mech.* **2000**, *22*, 222–226. (In Chinese with English Abstract). [CrossRef]
42. Liu, J.; Wang, S.; Yang, H. Method to determine the rheological tesy long-term strength for soft intercalations. *Site Investig. Sci. Technol.* **1996**, *14*, 3–7. (In Chinese)
43. Wang, Y.; Li, J.; Liu, F. Experimental research on shear creep and its long-term strength of weak intercalation in dam foundation. *Chin. J. Rock Mech. Eng.* **2013**, *32*, 3378–3384. (In Chinese with English Abstract). Available online: https://kns.cnki.net/kcms2/article/abstract?v=3uoqIhG8C44YLTlOAiTRKjw8pKedNdX5_mkCYmAjR9woATR5jJrIuB6lTzqRtYl4mVxrA3cn7SqNHpb4CzoR2GVXgnlnCsYb&uniplatform=NZKPT (accessed on 29 May 2012).
44. Gu, D. *Foundations of Engineering Geomechanics of Rock Mass*; Science Press: Beijing, China, 1979.

45. Zhu, S.; Yin, Y.; Li, B. Shear creep behavior of soft interlayer in Permian carbonaceous shale. *Rock Soil Mech.* **2019**, *40*, 1377–1386. (In Chinese with English Abstract) [CrossRef]
46. Chen, Q.; Zhou, D.; Feng, Z. Research on the Shear Creep Property of a Typical Weak Intercalation in Redbed Soft Rock. *Chin. J. Rock Mech. Eng.* **2009**, *28*, 3176–3180. (In Chinese with English Abstract) [CrossRef]